



Polarization Measurement Method Based on Liquid Crystal Variable Retarder (LCVR) for Atomic Thin-Film Thickness

Yucong Yuan¹ · Chengyuan Yao¹ · Wanfu Shen¹ · Xiaodong Hu¹ · Chunguang Hu¹

Received: 20 December 2021 / Revised: 1 February 2022 / Accepted: 8 February 2022 / Published online: 6 April 2022
© The Author(s) 2022

Abstract

Atomic thickness thin films are critical functional materials and structures in atomic and close-to-atomic scale manufacturing. However, fast, facile, and highly sensitive precision measurement of atomic film thickness remains challenging. The reflected light has a dramatic phase change and extreme reflectivity considering the Brewster angle, indicating the high sensitivity of the optical signal to film thickness near this angle. Hence, the precision polarization measurement method focusing on Brewster angle is vital for the ultrahigh precision characterization of thin films. A precision polarization measurement method based on a liquid crystal variable retarder (LCVR) is proposed in this paper, and a measurement system with a high angular resolution is established. A comprehensive measurement system calibration scheme is also introduced to accommodate ultrahigh precision film thickness measurement. Repeatable measurement accuracy to the subnanometer level is achieved. Standard silicon oxide film samples of different thicknesses were measured around Brewster angle using the self-developed system and compared with a commercial ellipsometer to verify the measurement accuracy. The consistency of the thickness measurement results demonstrates the feasibility and robustness of the measurement method and calibration scheme. This study also demonstrates the remarkable potential of the LCVR-based polarization method for atomic film thickness measurement in ultraprecision manufacturing.

Keywords Atomic thickness thin film · Thickness · Polarization measurement · Brewster angle · LCVR

1 Introduction

Thin films play an important role in the fields of semiconductors [1, 2], new energy [3, 4], and biomedicine [5, 6], and new demands and challenges for high-precision manufacturing of thin films are continuously raised. As the processing scale approaches from the micron and nanometer to the atomic level, modern manufacturing technology will move toward atomic and close-to-atomic scale manufacturing (ACSM) [7, 8]. Atomic thickness films are the crucial basic materials and structures that connect microscopic functional modules to macroscopic systems. Atomic thickness variations can induce remarkable changes in material properties or processing when the film thickness is below sub-hundred

nanometers. Hence, accurate measurement of atomic film thickness not only benefits the determination of the apparent physicochemical properties of the material but also is a critical parameter indicator and production benchmark for ultraprecision manufacturing. Precision measurement methods for the ultrathin film thickness of nanomaterials currently include scanning probe microscopy (atomic force and scanning tunneling microscopy), electron beam microscopy (scanning/transmission electron microscopy and low-energy electron diffractometer), and optical measurement methods (spectroscopic ellipsometry, reflectance spectroscopy, and Raman spectroscopy). The first two categories are surface characterization methods commonly used in surface physics and nanoscience. Measuring the internal or subsurface conditions of the film layer using scanning probe microscopy, which focuses on surface topography, is difficult; the scanning speed is slow, and the measuring area is small [9, 10]. Electron beam microscopy has high surface sensitivity, but the sample preparation procedure is sophisticated and requires a high-vacuum atmosphere for measurement, which is expensive and time-consuming [11–13]. The

✉ Chengyuan Yao
yaochengyuan@tju.edu.cn

✉ Chunguang Hu
cghu@tju.edu.cn

¹ State Key Laboratory of Precision Measuring Technology and Instruments, Tianjin University, Tianjin 300072, China

optical method provides lateral submicron and longitudinal subnanometer measurement resolutions and benefits from noncontact, nondestructive, and low environmental requirements, making it ideal for measuring atomic thickness thin-film samples [14–17].

Among optical methods, spectroscopic ellipsometry is the classical, highly accurate, and widespread technique for thin-film thickness measurement. Moreover, LCVR has been widely utilized in phase modulation ellipsometry due to the advantages of mechanical motion absence, fast response speed, compact structure, and low cost [18, 19]. Conventional variable angle spectroscopic ellipsometry (VASE) is performed over a large range of incidence angles and at relatively low incidence angle resolution. The effective thickness of atomic films is typically below sub-hundred nanometers, and the ultrashort optical range causes weak changes in light intensity and phase. A thin thickness weakens the amount of light intensity signal change and rapidly declines signal-to-noise ratio and film thickness measurement sensitivity. Consequently, the VASE must be optimized to enhance the accuracy and sensitivity for atomic-level thickness films. Notably, the contrast ratio of single-layer graphene imaging has been boosted over 300 times based on the developed Brewster angle oblique incidence optical microscopy technique [20]. Quality assessment of the machined surface is accomplished by detecting the change in the phase difference of the reflected light adjacent to the Brewster angle for polished hard and brittle crystals [21]. The above approaches adequately reveal the high sensitivity of the optical signal to film thickness near the Brewster angle. Compared with conventional ellipsometry, polarization signal measurement is performed by selecting the Brewster angle region, which is sensitive to thickness. The method is essentially an optimized measurement scheme for atomic film thickness based on spectroscopic ellipsometry. The method aims to increase the proportion of reflected film information in the overall reflected light intensity while restraining the substrate reflected signal, thus improving the thickness measurement sensitivity. Thus, the method is a prospective optical measurement technique that can satisfy the future demand for high-precision measurement in ultraprecision manufacturing.

A precision polarization measurement method for atomic film thickness in the vicinity of Brewster angle is chosen in this paper based on liquid crystal variable retarder (LCVR). A film thickness measurement system with high angular resolution in the narrow range of incidence angles near Brewster angle is developed. Systematic calibration schemes are also designed for the core polarization optics to satisfy high accuracy measurement requirements. Multiple silicon oxide thin-film samples of different thicknesses were measured with repeatable measurement accuracy to the subnanometer level for demonstration. The consistency with the thickness

measurement results of the commercial ellipsometer verifies the feasibility and robustness of the measurement method and calibration scheme. Overall, an atomic film thickness measurement scheme with high sensitivity and accuracy, which provides a powerful approach for thin-film characterization in ACSM, is proposed.

2 Instrumentation and Measurement Principle

Figure 1 shows the proposed LCVR-based precision polarization measurement scheme for atomic thin-film thickness with PLSA configuration of ellipsometry structure. The incident angle adjustment is realized by synchronous rotation of the incident and reflective optical path arms driven by the motorized rotary mechanism. The range of the incident angle is 30° – 90° , and the angular resolution is 0.02° . The nominal wavelength of the diode laser source (Coherent, OBIS 640 nm LX40) is 640 nm, and the output power is 40 mW. The laser passes through a linear polarizer (Thorlabs, GTH10M-A) and an LCVR (Thorlabs, LCC1223T-A) successively and then strikes the surface of the sample. The incident light is reflected by the sample and converted from linearly polarized light with a known polarization state to elliptically polarized light carrying information regarding the sample. The reflected light is captured by the detector (Thorlabs, PDA100A2) after crossing the analyzer (Thorlabs, GTH10M-A). The electrical signal is then collected by the data acquisition card and transmitted to the computer. The polarizer, LCVR, and analyzer are mounted on computer-controlled continuously rotatable motors for calibration procedures and azimuth-dependent polarization measurement. The fixed output power laser can be used with a variable neutral density filter to achieve tunable incident laser power, thus ensuring a high signal-to-noise ratio when measuring smooth and rough surface samples. The adopted LCVR is temperature-controlled to avoid the phase modulation error

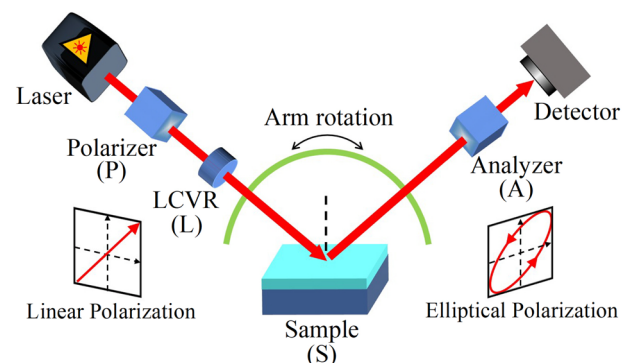


Fig. 1 LCVR-based precision polarization measurement scheme for atomic film thickness

due to temperature fluctuation [22]. A self-developed software system implements the hardware control of the instrument and the data analysis and processing functions.

Ellipsometry is an indirect measurement method. The optical constants and thicknesses are derived from the mathematical inversion of the ellipsometry parameters (ψ, Δ) by establishing an optical model corresponding to the thin-film sample. The expression for the received light intensity of the detector shown in Fig. 1 based on the Mueller matrix is as follows [23]:

$$I_{out} = R(-\alpha_A) \cdot A \cdot R(\alpha_A) \cdot S \cdot R(-\alpha_L) \cdot L \cdot R(\alpha_L) \cdot R(-\alpha_p) \cdot P \cdot R(\alpha_p) \cdot I_{in}, \tag{1}$$

where I_{in} is the Stokes vector of the incident light, and R is the Mueller rotation matrix. $P, L, S,$ and A are the Mueller matrices of the polarizer, LCVR, sample, and analyzer, respectively, assuming the absence of depolarization effect and the sample is isotropic. $\alpha_p, \alpha_L,$ and α_A are the azimuth angles of the polarizer, LCVR, and analyzer, correspondingly. The Stokes vector and the Mueller matrices are given in reference [23].

$\alpha_p, \alpha_L,$ and α_A are $45^\circ, 0^\circ,$ and $45^\circ,$ respectively, during measurement, and Eq. (1) is simplified to the following expression:

$$I_{out} = I_0[1 + \cos(\delta + \Delta) \cdot \sin(2\psi)], \tag{2}$$

where I_0 is the incident light intensity, which is considered constant during the measurement; δ is the phase retardation of LCVR, which is modulated by the control voltage. ψ and Δ are the ellipsometry parameters of the sample. Equation (2) reveals the existence of three unknowns, namely $I_0, \psi,$ and $\Delta,$ when the LCVR phase retardation δ is known. Therefore, the ellipsometry parameters (ψ, Δ) of the sample can be derived when the light intensity values corresponding to the three-phase retardations are acquired separately. ψ and Δ are calculated in accordance with the light intensity $I_{\delta=60}, I_{\delta=90},$ and $I_{\delta=120}$ corresponding to the phase retardation δ of $60^\circ, 90^\circ,$ and $120^\circ,$ respectively, and the equation is as follows:

$$\begin{cases} X = \frac{I_{\delta=60} + I_{\delta=120} - 2I_{\delta=90}}{I_{\delta=60} + I_{\delta=120}} = (2 - \sqrt{3}) \tan(\Delta) \\ Y = \frac{I_{\delta=60} - I_{\delta=120}}{I_{\delta=60} + I_{\delta=120} - \sqrt{3}I_{\delta=90}} = (2 + \sqrt{3}) \cos(\Delta) \sin(2\psi) \end{cases} \tag{3}$$

$$\begin{cases} \Delta = \arctan\left(\left(2 + \sqrt{3}\right)X\right) \\ \psi = 0.5 \arcsin\left(\left(2 - \sqrt{3}\right)Y / \cos \Delta\right) \end{cases}$$

The thickness of the film can be determined by Fresnel’s formula based on the measured ellipsometry parameters (ψ, Δ) through data inversion when the optical constants of the ambient medium, the film, and the substrate are known [23].

3 Calibration Method

A systematic calibration scheme is indispensable to guarantee the accuracy and repeatability of thin-film thickness measurements. The polarization optics in the measurement system must be fixed at a specific azimuth angle during the measurement; thus, the azimuth must be precisely aligned. The phase retardation δ of the LCVR is determined by the incident wavelength and control voltage. Therefore, the calibration of the LCVR retardation versus control voltage is required. Overall, a systematic scheme is proposed for the above calibration demands.

3.1 Polarizer Azimuth Angle Calibration

The reference for the azimuth angle of all optics is the incident plane. Hence, the polarization transmission direction of the linear polarizer should be first calibrated corresponding to the incident plane. The azimuth angle of the LCVR and the analyzer is referenced to the transmission direction of the polarizer, thus ensuring the consistency of the reference. Herein, only the light source, the polarizer, the sample, and the detector are in the optical measurement path, and the incident angle is adjacent to the Brewster angle of the sample. Therefore, the light intensity received by the detector is shown in Eq. (4).

$$I_{out} = S \cdot R(-\alpha_p) \cdot P \cdot R(\alpha_p) \cdot I_{in} = I_0(1 - \cos(2\alpha_p) \cos(2\psi)). \tag{4}$$

The p-polarized light in the reflected light disappears when the incident angle is Brewster angle, and then ψ is zero. The light intensity is minimum and maximum at this time when the polarization transmission direction of the polarizer is parallel to the incident plane ($\alpha_p = 0^\circ/180^\circ$) and perpendicular to the incident plane ($\alpha_p = \pm 90^\circ$), respectively. Therefore, the $0^\circ/90^\circ$ azimuth angle of the polarizer considering the incident plane can be determined by searching for the extremes of the light intensity. A high-precision rotating motor can then be used to position the polarizer at any azimuth angle precisely. However, the above calibration methodology is “infeasible” because it is virtually impossible to align the incident angle to the Brewster angle rigorously due to the positioning accuracy of the instrument hardware. Nevertheless, combined with Eq. (4), the above conclusion of light intensity change remains valid when

ψ is in the range of 0–45° (the angle of incidence is near Brewster angle). Therefore, the variation of light intensity in the vicinity of the Brewster angle is simulated with the azimuth angle of the polarizer, as shown in Fig. 2. The incident intensity is the normalized natural light source, and ψ varies from 0 to 45° in steps of 1°. The azimuth angle of the polarizer varies from –180° to 180° in steps of 5°. Figure 2a shows that the amplitude of the reflected light intensity curve is larger when ψ is less than 35° and small in the range of 35–45°. This result guides the incident angle selection during calibration. Meanwhile, the azimuth angle of the polarizer can be calibrated in the vicinity of the Brewster angle (the incident angle does not need to be rigorously Brewster angle), demonstrating the robustness of the calibration method. Fitting the sine curve of the polarizer azimuth angle and the light intensity near the light intensity maximum is necessary to obtain the 90° azimuth angle of the polarizer accurately.

3.2 Analyzer and LCVR Azimuth Angle Calibration

The polarizer is rotated to 45° as a reference for the subsequent azimuth alignment of the analyzer and LCVR based on its azimuth calibration. The VASE system is then rotated to the straight-through mode with an incidence angle of 90°. The analyzer is inserted into the optical path, and the light intensity is shown in Eq. (5).

$$I_{out} = R(-\alpha_A) \cdot A \cdot R(\alpha_A) \cdot R(-\alpha_P) \cdot A \cdot R(\alpha_P) \cdot I_{in} = 2I_0 \cos^2(\alpha_A - \alpha_P) \tag{5}$$

Equation (5) reveals that the light intensity is maximum and minimum when the analyzer is respectively parallel and perpendicular to the polarizer. Afterward, the polarizer and analyzer are rotated perpendicular, and the LCVR is added to the optical path. The light intensity is shown in Eq. (6).

$$I_{out} = R(-\alpha_A) \cdot A \cdot R(\alpha_A) \cdot R(-\alpha_L) \cdot L \cdot R(\alpha_L) \cdot R(-\alpha_P) \cdot P \cdot R(\alpha_P) \cdot I_{in} \tag{6}$$

$\alpha_A - \alpha_P = 90^\circ$ is substituted into Eq. (6) and simplified to obtain Eq. (7).

$$I_{out} = 0.5I_0[(1 - 2 \cos \delta) \cdot \sin^2(2\alpha_P - 2\alpha_L)] \tag{7}$$

Equation (7) shows that the minimum of light intensity is achieved when the LCVR is parallel or perpendicular to the azimuth angle of the polarizer and the control voltage is fixed. Herein, the two cases are distinguished by observing the polarization transmission direction marker on the LCVR housing.

3.3 LCVR Retardation Calibration

The azimuth angles of the polarizer and LCVR in the straight-through mode are fixed at 45° and 0°, respectively. Assuming the light intensity of the source is constant during the measurement, the detected light intensities $I_{\alpha_A=45}$, $I_{\alpha_A=-45}$ at the azimuth angle of the analyzer of $\pm 45^\circ$ are measured as shown in Eq. (8).

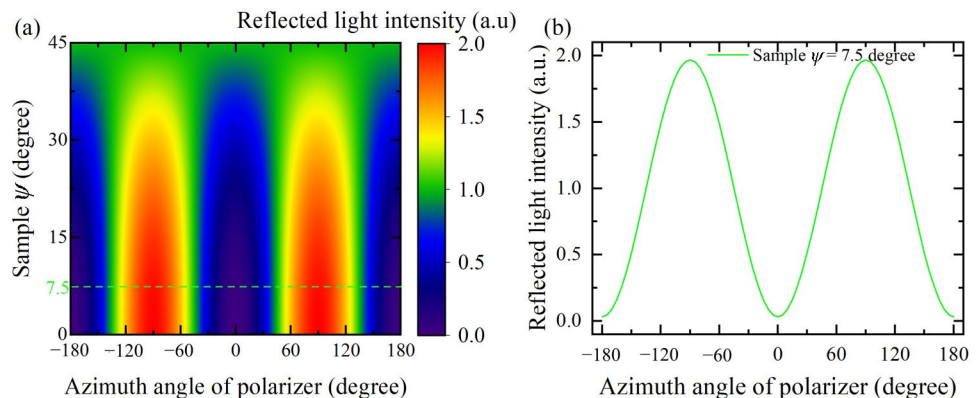
$$I_{\alpha_A=45} = I_0(1 + \cos \delta), \quad I_{\alpha_A=-45} = I_0(1 - \cos \delta) \tag{8}$$

Therefore, the retardation of the LCVR, δ , is then given by Eq. (9).

$$\delta = \arccos\left(\frac{I_{\alpha_A=45} - I_{\alpha_A=-45}}{I_{\alpha_A=45} + I_{\alpha_A=-45}}\right) \tag{9}$$

The above procedure indicates that the calibration of the LCVR phase retardation δ corresponding to the control voltage is accomplished by altering the control voltage. The calibration of δ within 4–20 V for the LCVR control voltage used in this paper is shown in Fig. 3.

Fig. 2 **a** Reflected light intensity considering different ψ and the azimuth angle of the polarizer; **b** Reflected light intensity curve with the azimuth angle of the polarizer at $\psi = 7.5^\circ$



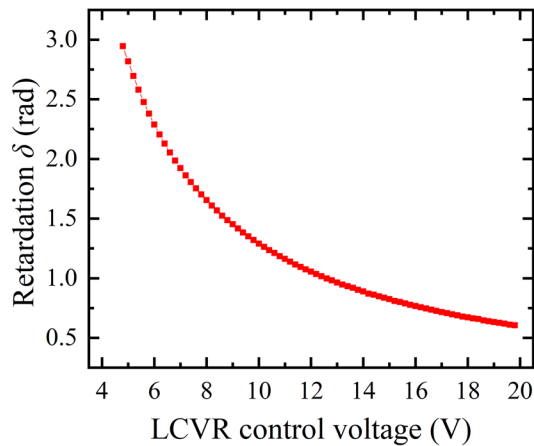


Fig. 3 LCVR retardation δ calibration curve

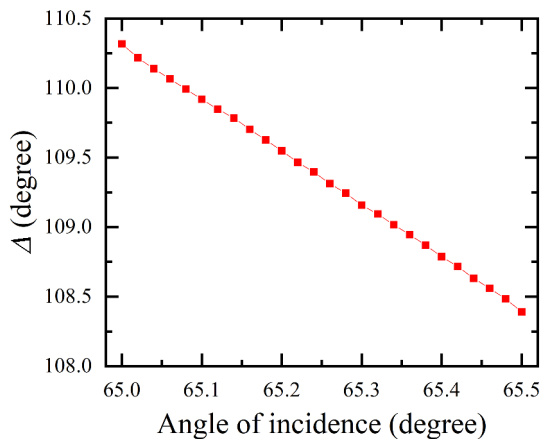


Fig. 4 Incident angle resolution measurement results

4 Results and Discussion

The high angular resolution of the variable incidence angle mechanism must be guaranteed to obtain dramatic changes in ψ and Δ in narrow angular ranges accurately. Therefore, the phase difference Δ curve of a silicon oxide thin-film sample with a nominal thickness of 60 nm was measured with the self-developed system, as shown in Fig. 4. The incident angle range is 65–65.5° in 0.02° steps, the measurement is repeated ten times, and the average value is taken as the final result. The distinct difference in the Δ at 0.02° intervals demonstrates that the incident angle resolution reaches 0.02°, fulfilling the need for polarization measurements with high incident angle resolution dependence near Brewster angle.

The system is calibrated using the above calibration procedures to ensure accuracy before measurement. Three samples with a nominal thickness of 2, 10, and 60 nm for silicon oxide film on a silicon substrate were measured, as shown in

Fig. 5a. Figure 5b, c show the curves of ellipsometry parameters (ψ and Δ) with the incident angle for the three samples, respectively. The incidence angle varies from 72° to 78° in steps of 0.1°. The ψ and Δ curves of different samples have significant variations. The trend of ψ and Δ around Brewster angle is smooth when the film is thick. The result reveals that the ψ , Δ near the Brewster angle have superior sensitivity to the atomic film thickness compared with other incidence angle ranges. The comparison of Fig. 5b, c shows that the sensitivity of the phase difference Δ is considerably higher than that of the amplitude ratio ψ , which is appropriate for detecting changes in the thickness of atomic thin films. The sensitivity of the measured signal near the Brewster angle is high when the film thickness is less than 60 nm. Moreover, the sensitivity is high when the thickness is small, which is determined by the nature of the phase jump at the Brewster angle. Importantly, this thickness value is not fixed and is dependent on the material type and the film layer structure.

A three-phase model of “air/silicon oxide film/silicon substrate” is built, and the film thickness is derived by fitting the measurement data. The Levenberg–Marquardt method is exploited for measurement data fitting [24]. The laser output is centered at 640 nm and calibrated by a precision spectrometer (Ocean Optics, QE65Pro). The optical constants of silicon oxide film and substrate are from [25, 26]. The film thickness repeatability measurement results are shown in Fig. 6 for each sample repeated ten times. Repeatability measurements were performed at a temperature of 26 ± 0.5 °C, and the single measurement time was approximately 2 min. Samples were fixed to ensure the consistency of the measurement region. The repeatability of the film thickness measurement reaches the subnanometer level, indicating the feasibility and robustness of the measurement principle and calibration method. The difference in the film thickness may be attributed to the fluctuation of the light source power, the instability of the LCVR control voltage, and the detector noise.

The samples were individually measured using a commercial ellipsometer (J.A. Woollam, RC2) to further illustrate the accuracy of the measurement results, and the results were compared with the self-developed system measurements as shown in Table 1. The measurement accuracy of the commercial ellipsometer is 0.01 nm (standard deviation of 30 measurements of a 2-nm naturally oxidized SiO₂ layer), and the film thickness measurement range is 1–10 μm (SiO₂ film on Si substrate). The measurement results are consistent, and differences in thickness may be related to changes in the measurement regions of the samples. The accuracy and robustness of the measurement system are guaranteed due to the proposed system calibration procedure. Meanwhile, the high-precision measurement capability of the LCVR-based precision polarization measurement method near Brewster angle for atomic thin-film thickness

Fig. 5 **a** Photograph of the standard samples. **b, c** Curves of the sample ellipsometry parameters ψ and Δ with the incident angle, respectively

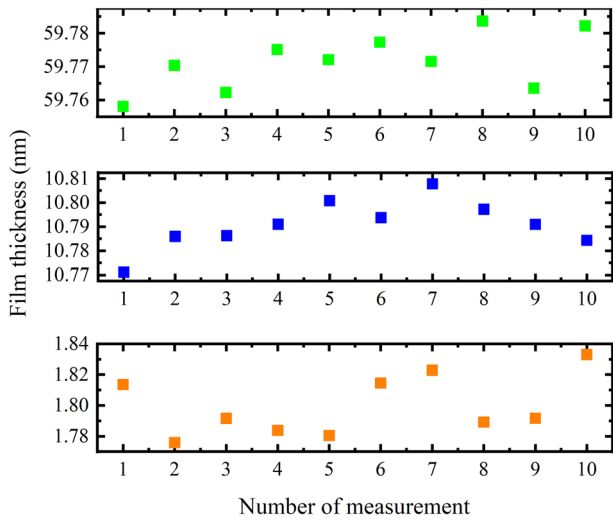
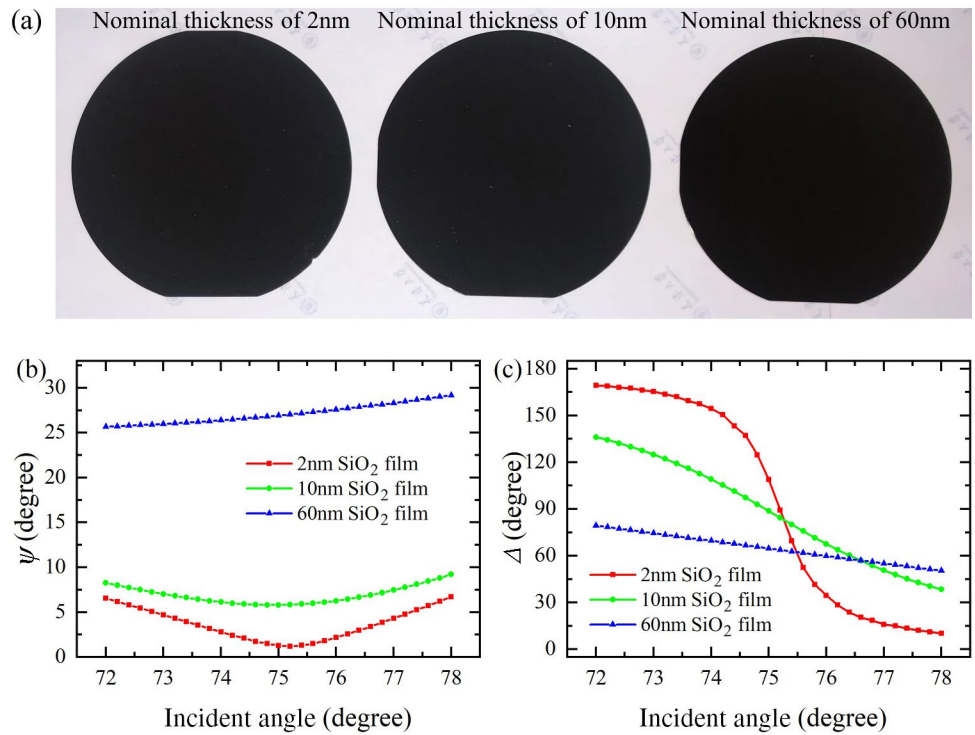


Fig. 6 Repeatability measurement results for film thickness

Table 1 Comparison with commercial ellipsometer film thickness measurement results

Nominal value (nm)	Commercial ellipsometer (nm)	Self-developed system (nm)	Error (%)
2	1.85	1.80	2.78
10	10.60	10.79	-1.79
60	58.60	59.77	-1.99

is verified. Therefore, this study further expands the application potential of LCVR and breaks the perception that LCVR generally fails to achieve high-precision quantitative polarization optical measurements and can only be utilized for qualitative applications [27]. This study demonstrates the high sensitivity of film thickness measurements near the Brewster angle of the single-layer model. Moreover, the study has important potential for film thickness measurements in multilayer structures, and the applicability of the method must be further investigated.

5 Conclusions

The LCVR-based precision polarization measurement method for atomic film thickness near Brewster angle is proposed, and a prototype with a high angular resolution is built. A systematic calibration scheme is designed for the measurement system structure to ensure accuracy and robustness. Three silicon oxide thin-film samples with nominal thicknesses of 2, 10, and 60 nm were measured for demonstration. Repeatable measurement accuracy reaches subnanometer levels for different samples, indicating the capability for high-precision measurement of atomic thin-film sample thickness. Simultaneously, the measured thickness is consistent with the nominal value and verified by a commercial ellipsometer, indicating that the film thickness measurement capability of the LCVR-based polarization

measurement system is comparable to a commercial ellipsometer. Overall, a high-precision measurement method and a measurement system construction guide for atomic thin-film thickness, which provide a powerful approach to satisfy the urgent needs for high-precision characterization of ultrathin films in ACSM, are proposed.

Acknowledgements The project is supported by National Key Research & Development Program of China (Grant No. 2019YFB2005601), the General Program of NSFC (52075383) and Major Scientific Research Instrument Development Project of NSFC (61927808).

Declarations

Conflict of interest The authors declare that the research was conducted in the absence of any commercial or financial relationships that could be construed as a potential conflict of interest.

Open Access This article is licensed under a Creative Commons Attribution 4.0 International License, which permits use, sharing, adaptation, distribution and reproduction in any medium or format, as long as you give appropriate credit to the original author(s) and the source, provide a link to the Creative Commons licence, and indicate if changes were made. The images or other third party material in this article are included in the article's Creative Commons licence, unless indicated otherwise in a credit line to the material. If material is not included in the article's Creative Commons licence and your intended use is not permitted by statutory regulation or exceeds the permitted use, you will need to obtain permission directly from the copyright holder. To view a copy of this licence, visit <http://creativecommons.org/licenses/by/4.0/>.

References

- Cai W, Li H, Zang Z (2021) One-volt, solution-processed InZnO thin-film transistors. *IEEE Electron Device Lett* 42:525–528
- Fortunato E, Barquinha P, Martins R (2012) Oxide semiconductor thin-film transistors: a review of recent advances. *Adv Mater* 24:2945–2986
- Büttner P, Scheler F, Pointer C, Döhler D, Yokosawa T, Spiecker E, Boix PP, Young ER, Mínguez-Bacho I, Bachmann J (2021) ZnS ultrathin interfacial layers for optimizing carrier management in Sb_2S_3 -based photovoltaics. *ACS Appl Mater Interfaces* 13:11861–11868
- Raiford JA, Oyakhire ST, Bent SF (2020) Applications of atomic layer deposition and chemical vapor deposition for perovskite solar cells. *Energy Environ Sci* 13:1997–2023
- Blendinger F, Seitz D, Ottenschläger A, Fleischer M, Bucher V (2021) Atomic layer deposition of bioactive TiO_2 thin films on polyetheretherketone for orthopedic implants. *ACS Appl Mater Interfaces* 13:3536–3546
- de Almeida Bino MC, Eurídice WA, Gelamo RV, Leite NB, da Silva MV, de Siervo A, Pinto MR, de Almeida Buranello PA, Moreto JA (2021) Structural and morphological characterization of Ti6Al4V alloy surface functionalization based on Nb_2O_5 thin film for biomedical applications. *Appl Surf Sci* 557:149739
- Fang FZ, Zhang N, Guo D, Ehmann K, Cheung B, Liu K, Yamamura K (2019) Towards atomic and close-to-atomic scale manufacturing. *Int J Extreme Manuf* 1:012001
- Gao J, Luo X, Fang FZ, Sun J (2021) Fundamentals of atomic and close-to-atomic scale manufacturing: a review. *Int J Extreme Manuf* 4:012001
- Corbett JP, Zhu T, Ahmed AS, Tjung SJ, Repicky JJ, Takeuchi T, Guerrero-Sanchez J, Takeuchi N, Kawakami RK, Gupta JA (2020) Determining surface terminations and chirality of noncentrosymmetric FeGe thin films via scanning tunneling microscopy. *ACS Appl Mater Interfaces* 12:9896–9901
- Korolkov VV, Summerfield A, Murphy A, Amabilino DB, Watanabe K, Taniguchi T, Beton PH (2019) Ultra-high resolution imaging of thin films and single strands of polythiophene using atomic force microscopy. *Nat Commun* 10:1537
- Kuhrau S, Kloodt-Twesten F, Heyn C, Oepen HP, Frömter R (2018) Cap-layer-dependent oxidation of ultrathin cobalt films and its effect on the magnetic contrast in scanning electron microscopy with polarization analysis. *Appl Phys Lett* 113:172403
- Teodorescu CM, Pintilie L, Apostol NG, Costescu RM, Lungu GA, Hrib L, Trupină L, Tănase LC, Bucur IC, Bociunea AE (2017) Low-energy electron diffraction from ferroelectric surfaces: dead layers and surface dipoles in clean $\text{Pb}(\text{Zr}, \text{Ti})\text{O}_3(001)$. *Phys Rev B* 96:115438
- Yun H, Ganguly K, Postiglione W, Jalan B, Leighton C, Mkhoyan KA, Jeong JS (2018) Microstructure characterization of BaSnO_3 thin films on LaAlO_3 and PrScO_3 substrates from transmission electron microscopy. *Sci Rep* 8:10245
- Emam-Ismail M, El-Hagary M, Shaaban ER, Moustafa SH, Gad GMA (2019) Spectroscopic ellipsometry and morphological characterizations of nanocrystalline $\text{Hg}_{1-x}\text{Mn}_x\text{O}$ oxide diluted magnetic semiconductor thin films. *Ceram Int* 45:8380–8387
- Huo S, Wang H, Hu C, Yao C, Shen W, Hu X, Hu X (2021) Measuring the multilayer silicon-based microstructure using differential reflectance spectroscopy. *Opt Express* 29:3114–3122
- Kraynis O, Makagon E, Mishuk E, Hartstein M, Wachtel E, Lubomirsky I, Livneh T (2019) Suitability of Raman spectroscopy for assessing anisotropic strain in thin films of doped ceria. *Adv Funct Mater* 29:1804433
- Tang Y, Chiabrera F, Morata A, Garbayo I, Alayo N, Tarancón A (2021) Pushing the study of point defects in thin film ferrites to low temperatures using in situ ellipsometry. *Adv Mater Interfaces* 8:2001881
- López-Téllez JM, Bruce NC (2014) Mueller-matrix polarimeter using analysis of the nonlinear voltage–retardance relationship for liquid-crystal variable retarders. *Appl Opt* 53:5359–5366
- Bruce NC, López-Téllez JM, Rodríguez-Núñez O, Rodríguez-Herrera OG (2018) Permitted experimental errors for optimized variable-retarder Mueller-matrix polarimeters. *Opt Express* 26:13693–13704
- Romagnoli P, Rosa HG, Lopez-Cortes D, Souza EAT, Viana-Gomes JC, Margulis W, de Matos CJS (2015) Making graphene visible on transparent dielectric substrates: Brewster angle imaging. *2D Mater* 2:035017
- Yao C, Huo S, Shen W, Sun Z, Hu X, Hu X, Hu C (2021) Assessing the quality of polished brittle optical crystal using quasi-Brewster angle technique. *Precis Eng* 72:184–191
- Hu C, Xie P, Huo S, Li Y, Hu X (2014) A liquid crystal variable retarder-based reflectance difference spectrometer for fast, high precision spectroscopic measurements. *Thin Solid Films* 571:543–547
- Fujiwara H (2007) Spectroscopic ellipsometry: principles and applications. Wiley, New Jersey
- Liu Y, Qiu J, Liu L, Cao B (2019) Extracting optical constants of solid materials with micro-rough surfaces from ellipsometry without using effective medium approximation. *Opt Express* 27:17667–17680
- Rodríguez-de Marcos LV, Larruquert JI, Méndez JA, Aznárez JA (2016) Self-consistent optical constants of SiO_2 and Ta_2O_5 films. *Opt Mater Express* 6:3622–3637
- Schinke C, Christian Peest P, Schmidt J, Brendel R, Bothe K, Vogt MR, Kröger I, Winter S, Schirmacher A, Lim S, Nguyen HT,

- MacDonald D (2015) Uncertainty analysis for the coefficient of band-to-band absorption of crystalline silicon. *AIP Adv* 5:067168
27. Bass M, DeCusatis C, Enoch J, Lakshminarayanan V, Li G, Macdonald C, Mahajan V, Stryland EV (2010) *Handbook of optics: volume I-geometrical and physical optics, polarized light, components and instruments*. McGraw-Hill, New York